

# Stable computation of the functional variation of the Dirichlet–Neumann operator

Carlo Fazioli, David P. Nicholls \*

*Department of Mathematics, Statistics, and Computer Science, University of Illinois at Chicago, Chicago, IL 60607, United States*

## ARTICLE INFO

### Article history:

Received 9 March 2009

Received in revised form 24 September 2009

Accepted 13 October 2009

Available online 17 October 2009

### Keywords:

Dirichlet–Neumann operators

Functional variations

Boundary Perturbation methods

High-order/spectral methods

Water waves

## ABSTRACT

This paper presents an accurate and stable numerical scheme for computation of the first variation of the Dirichlet–Neumann operator in the context of Euler's equations for ideal free-surface fluid flows. The Transformed Field Expansion methodology we use is not only numerically stable, but also employs a spectrally accurate Fourier/Chebyshev collocation method which delivers high-fidelity solutions. This implementation follows directly from the authors' previous theoretical work on analyticity properties of functional variations of Dirichlet–Neumann operators. These variations can be computed in a number of ways, but we establish, via a variety of computational experiments, the superior effectiveness of our new approach as compared with another popular Boundary Perturbation algorithm (the method of Operator Expansions).

© 2009 Elsevier Inc. All rights reserved.

## 1. Introduction

Boundary operators such as the Dirichlet–Neumann operator (DNO) appear in many models of physical phenomena, including free-surface fluid mechanics [1], and acoustic and electromagnetic scattering [2,3]. These operators are important as they typically permit the restatement of the governing equations at the *boundary* of the domain on which the problem is posed. This reduction in dimension is clearly advantageous from both theoretical and numerical points of view and has, therefore, been pursued by a number of authors. In the particular example of open-ocean free-surface flows (the water wave problem) which we consider here, the governing Euler equations [4] can be recast as evolution equations for the shape of the free-surface and the velocity potential at the surface, as shown by Zakharov [5] and Craig and Sulem [1].

In many applications it is necessary to compute the variation of the DNO with respect to the boundary shape. For example, one of the authors [6,7] utilized a Newton's method in a continuation algorithm for locating traveling wave solutions of the water wave problem. Alternatively, in a linear stability analysis of solutions of the water wave problem, the variation of the DNO must be computed to estimate the linearized water wave operator [8,9]. Despite the importance of these applications, very little has been accomplished in the development of algorithms for approximating variations of the DNO. In this paper we present, for the first time, a stable and high-order numerical scheme for their computation.

Many algorithms are available for the simulation of boundary operators such as the DNO. Methods based upon integral equations, finite differences, and finite elements are all available, however, if the shape of the geometry is a small deformation of a simple one (e.g., a separable domain such as a rectangle in two dimensions) then an algorithm based upon perturbation series is natural. For the computation of DNO, several Boundary Perturbation algorithms are available including the methods of Operator Expansions (OE) [1,10–15], Field Expansions (FE) [16–22], and Transformed Field Expansions (TFE)

\* Corresponding author. Tel.: +1 312 413 1641; fax: +1 312 996 1491.

E-mail addresses: [cxfazioli@math.uic.edu](mailto:cxfazioli@math.uic.edu) (C. Fazioli), [nicholls@math.uic.edu](mailto:nicholls@math.uic.edu) (D.P. Nicholls).

[23–25]. The former two methods are easy to implement, highly accurate within their domain of applicability (e.g., the excellent agreement between the numerical simulations of [13,15] and wave tank experiments), and have computational complexity competitive with state-of-the-art integral equation solvers [26]. However, these methods can become unstable when applied to domains which are large and/or irregular deformations of the simple geometry. Not only was this behavior explicitly demonstrated in [23–25], but also a new approach, precisely the TFE method mentioned above, was developed to overcome these shortcomings and then verified to be stable and highly accurate.

In addition to the numerical stability properties of the TFE recursions, they can also be used to place the theory of functional variations of boundary operators on a solid footing [27]. In particular, the boundary flattening change of variables which constitutes the first step of the TFE analysis immediately removes the boundary shape from the specification of the domain to the inhomogeneity of the governing differential equations. At this point a functional variation with respect to this boundary deformation is now a simple exercise in functional calculus utilizing nothing more sophisticated than the product rule.

In this contribution we will show that the numerical stability and accuracy properties of the TFE algorithm which were demonstrated for the computation of DNO [23–25] can be extended to their functional variations. While similar in spirit to this previous work, there are some significant new algorithmic challenges which must be overcome. For instance, the additional computational complexity and memory requirements associated to not only computing and storing the field and DNO (necessary for computing their variation, see (20) and (21)), but also the more involved inhomogeneities associated to the first variation; see again (20) and (21). Additionally, this new algorithm is, to the authors' knowledge, the *only* existent method for the stable and high-order computation of variations of the DNO.

The rest of the paper is organized as follows: The Euler equations of free-surface fluid mechanics and the role of the DNO in a surface formulation of these equations is given in Section 2. In Section 3 we present two Boundary Perturbation methods for the computation of DNO and their first variations, the method of Operator Expansions (fully described in Section A), and our new Transformed Field Expansions (Section 3.1). In Section 4 we outline our numerical method, Section 4.1, and present new numerical results in Section 4.2 which demonstrate the advantageous convergence properties of our new algorithm. Concluding remarks are given in Section 5.

## 2. Governing equations

The free-surface Euler equations constitute a model for the evolution of a large body of water (e.g., an ocean or lake), assumed to be an ideal fluid, under the influence of gravity (effects of capillarity can easily be incorporated if desired). For a precise statement, consider the domain

$$S_{h,\eta} := \{(x, y) \in \mathbf{R}^{d-1} \times \mathbf{R} \mid -h < y < \eta(x, t)\},$$

where  $h$  is the mean depth of fluid,  $d = 2, 3$  is the problem dimension, and  $\eta$  is the shape of the free-surface deformation from the rest state  $y = 0$ . The equations of motion (Euler equations) are [4]

$$\Delta\varphi = 0 \quad \text{in } S_{h,\eta}, \tag{1a}$$

$$\partial_y\varphi = 0 \quad \text{at } y = -h, \tag{1b}$$

$$\partial_t\eta - \partial_y\varphi + \nabla_x\eta \cdot \nabla_x\varphi = 0 \quad \text{at } y = \eta, \tag{1c}$$

$$\partial_t\varphi + \tilde{g}\eta + \frac{1}{2}|\nabla\varphi|^2 = 0 \quad \text{at } y = \eta, \tag{1d}$$

where  $\varphi$  is the velocity potential (the velocity is given by  $\vec{u} = \nabla\varphi$ ) and  $\tilde{g}$  is the gravitational constant. In the lateral direction we specify the classical periodic boundary conditions,

$$\varphi(x + \gamma, y, t) = \varphi(x, y, t), \quad \eta(x + \gamma, t) = \eta(x, t), \quad \forall \gamma \in \Gamma,$$

where  $\Gamma$  is a lattice in  $\mathbf{R}^{d-1}$ . This lattice  $\Gamma$  generates a conjugate lattice  $\Gamma'$  of wavenumbers (e.g., if  $\Gamma = \mathbf{LZ} \times \mathbf{MZ}$  then  $\Gamma' = (2\pi/L)\mathbf{Z} \times (2\pi/M)\mathbf{Z}$ ) thus providing a convenient and compact prescription of the Fourier series of a function, e.g.

$$f(x) = \sum_{k \in \Gamma'} \hat{f}_k e^{ik \cdot x},$$

where  $\hat{f}_k$  is the  $k$ th Fourier coefficient of  $f$ .

Zakharov [5] restated the problem (1) as a Hamiltonian system with the surface quantities  $\eta(x, t)$  and  $\zeta(x, t) := \varphi(x, \eta(x, t), t)$  as the canonical variables. Craig and Sulem [1] made this characterization much more explicit with the introduction of the Dirichlet–Neumann operator (DNO). To define the DNO, consider the rather generic elliptic problem inspired by (1)

$$\Delta v = 0 \quad \text{in } S_{h,g}, \tag{2a}$$

$$v(x, g(x)) = \zeta(x), \tag{2b}$$

$$\partial_y v(x, -h) = 0, \tag{2c}$$

$$v(x + \gamma, y) = v(x, y) \quad \forall \gamma \in \Gamma. \tag{2d}$$

Provided that  $g$  is sufficiently smooth (2) will have a unique solution whose normal derivative,  $v(x)$ , can be computed at the surface  $y = g$ . This mapping of the Dirichlet data  $\xi$  to Neumann data  $v$  is precisely the DNO which we denote

$$G(g)[\xi] := [\nabla v]_{y=g} \cdot N = \partial_y v(x, g(x)) - \nabla_x g \cdot \nabla_x v(x, g(x)), \tag{3}$$

where  $N = (1, -\nabla_x g)^T$  is an exterior normal. Given this definition of the DNO, a straightforward application of the chain rule transforms (1) to

$$\partial_t \eta = G(\eta)[\xi], \tag{4a}$$

$$\partial_t \xi = -\tilde{g}\eta - \frac{1}{2(1 + |\nabla_x \eta|^2)} \left[ |\nabla_x \xi|^2 - (G(\eta)[\xi])^2 - 2(\nabla_x \xi \cdot \nabla_x \eta)G(\eta)[\xi] + |\nabla_x \xi|^2 |\nabla_x \eta|^2 - (\nabla_x \xi \cdot \nabla_x \eta)^2 \right], \tag{4b}$$

c.f. [1].

Of course there are many interesting open questions regarding the theory and application of the model (4). One of these is the stability theory of periodic traveling wave solutions which has motivated the current contribution. To see how functional variations of the DNO arise in this context let us write (4) abstractly as

$$\partial_t u = F(u), \tag{5}$$

where  $u = (\eta, \xi)^T$ , and consider a periodic traveling wave solution  $u(x, t) = \bar{u}(x - ct)$ . One can investigate the dynamic stability of these traveling waves by considering the evolution of a small perturbation  $\tilde{u}$ :

$$u(x, t) = \bar{u}(x - ct) + \delta \tilde{u}(x, t), \quad \delta \ll 1.$$

Upon insertion of this form into (5) we see that this perturbation satisfies the evolution equation

$$\partial_t \tilde{u} = \delta_u F(\bar{u})[\tilde{u}] + \mathcal{O}(\delta). \tag{6}$$

Here,  $\delta_u F$  denotes the first functional variation of  $F$  “in the direction” of  $\tilde{u}$ , evaluated at the equilibrium point  $\bar{u}$ . If we ignore the  $\mathcal{O}(\delta)$  contributions (a linear stability analysis) and postulate that solutions have the form

$$\tilde{u}(x, t) = e^{it} w(x)$$

(a spectral stability analysis), then we can deduce stability properties of these traveling waves from the eigenproblem

$$\delta_u F(\bar{u})[w] = \lambda w.$$

We do not pursue this idea further in this paper, but we do point out that for our system (4), the first functional variation of the DNO is a *crucial* element of  $\delta_u F$  which must be faithfully simulated for a meaningful study of stability. The point of our paper is to provide an algorithm for exactly this purpose.

### 3. Boundary Perturbations

Having restated the Euler equations (1) in terms of surface variables (4) via the specification of Zakharov [5] and Craig and Sulem [1], a critical numerical concern is the robust computation of the DNO. Moreover, given that the first variation of the DNO arises in a number of important contexts (e.g., Newton’s method, spectral stability analysis), the accurate simulation of this operator is also of crucial importance. As we stated in Section 1, if the surface deformation is not too large then a perturbative method is natural and, as we shall see, can deliver highly accurate solutions in a robust fashion. In this section we consider two such algorithms, the “Operator Expansions” (OE) and “Transformed Field Expansions” (TFE) methods, which are amenable to the approximation of the both the DNO and its variation.

Before beginning, we note that the theorems of Calderón [28], Coifman and Meyer [29], Craig et al. [30], and Nicholls and Reitch [23] demonstrate that the DNO is analytic with respect to Boundary Perturbations so that the expansion

$$G(g)[\xi] = G(\varepsilon f)[\xi] = \sum_{n=0}^{\infty} G_n(f)[\xi] \varepsilon^n \tag{7}$$

converges strongly. Similarly, the authors showed in their previous work [27] that the first functional variation of the DNO

$$G^{(1)}(g)[\xi]\{w\} := \delta_g G(g)[\xi]\{w\} := \lim_{\tau \rightarrow 0} \frac{1}{\tau} (G(g + \tau w)[\xi] - G(g)[\xi])$$

is also analytic with respect to  $g$ , i.e.

$$G^{(1)}(g)[\xi]\{w\} = G^{(1)}(\varepsilon f)[\xi]\{w\} = \sum_{n=0}^{\infty} G_n^{(1)}(f)[\xi]\{w\} \varepsilon^n. \tag{8}$$

If we can find convenient formulas for the  $G_n$  and  $G_n^{(1)}$  (provided by the OE and TFE recursions) then highly accurate approximations of the DNO and its first variation can be given by, respectively

$$G^N(\varepsilon f)[\xi] := \sum_{n=0}^N G_n(f)[\xi] \varepsilon^n, \tag{9}$$

and

$$G^{(1,N)}(\varepsilon f)[\xi]\{w\} := \sum_{n=0}^N G_n^{(1)}(f)[\xi]\{w\} \varepsilon^n. \tag{10}$$

One popular Boundary Perturbation approach to the approximation of the  $G_n$  in the expansion of the DNO, Eq. (7), is the method of Operator Expansions (OE) due to Milder [10–12] and Craig and Sulem [1]. As this method has been fully elucidated in a number of publications (see the previous references and [24] for instance) we omit the details here and refer the interested reader to Appendix A. Included also in this appendix is the extension of this OE method to the computation of the first variation of DNO.

### 3.1. Transformed Field Expansions

The method of “Transformed Field Expansions” (TFE) follows a rather different philosophy than the OE method. We begin with a change of variables

$$x' = x, \quad y' = h \left( \frac{y - g(x)}{h + g(x)} \right), \tag{11}$$

which transforms the domain  $S_{h,g}$  to  $S_{h,0}$ . Furthermore, the transformed field quantity

$$u(x', y') := v \left( x', \frac{y'(h + g(x'))}{h} + g(x') \right),$$

satisfies, upon dropping primes,

$$\Delta u = F(x, y; g, u) \quad \text{in } S_{h,0}, \tag{12a}$$

$$u(x, 0) = \xi(x), \tag{12b}$$

$$\partial_y u(x, -h) = 0, \tag{12c}$$

$$u(x + \gamma, y) = u(x, y) \quad \forall \gamma \in \Gamma, \tag{12d}$$

where

$$F = \text{div}_x[F_x] + \partial_y F_y + F_h, \tag{12e}$$

and the  $x$ -derivative,  $y$ -derivative, and homogeneous parts of  $F$  are given by:

$$F_x = -\frac{2}{h} g \nabla_x u - \frac{1}{h^2} g^2 \nabla_x u + \frac{h+y}{h} \nabla_x g \partial_y u + \frac{h+y}{h^2} g \nabla_x g \partial_y u, \tag{12f}$$

$$F_y = \frac{h+y}{h} \nabla_x g \cdot \nabla_x u + \frac{h+y}{h^2} g \nabla_x g \cdot \nabla_x u - \frac{(h+y)^2}{h^2} |\nabla_x g|^2 \partial_y u, \tag{12g}$$

and

$$F_h = \frac{1}{h} \nabla_x g \cdot \nabla_x u + \frac{1}{h^2} g \nabla_x g \cdot \nabla_x u - \frac{h+y}{h^2} |\nabla_x g|^2 \partial_y u. \tag{12h}$$

Additionally, the DNO transforms to

$$G(g)[\xi] = \partial_y u(x, 0) + H(x; g, u), \tag{13a}$$

where

$$H = -\frac{1}{h} g G(g)[\xi] - \nabla_x g \cdot \nabla_x u(x, 0) - \frac{1}{h} g \nabla_x g \cdot \nabla_x u(x, 0) + |\nabla_x g|^2 \partial_y u(x, 0), \tag{13b}$$

c.f. [23]. The important fact about this particular gathering of terms is that  $F$  and  $H$  are  $\mathcal{O}(g)$ .

In this new set of variables the first variation of the DNO can be easily computed, though we also need to introduce the first variation of the (transformed) field  $u$  as well:

$$u^{(1)}(x, y; g)\{w\} := \delta_g u(x, y; g)\{w\} := \lim_{\tau \rightarrow 0} \frac{1}{\tau} (u(x, y; g + \tau w) - u(x, y; g)).$$

With a straightforward application of the product rule to (12) we find the following elliptic problem

$$\Delta u^{(1)} = F^{(1)}(x, y; g, w, u, u^{(1)}) \quad \text{in } S_{h,0}, \quad (14a)$$

$$u^{(1)}(x, 0) = 0, \quad (14b)$$

$$\partial_y u^{(1)}(x, -h) = 0, \quad (14c)$$

$$u^{(1)}(x + \gamma, y) = u^{(1)}(x, y) \quad \forall \gamma \in \Gamma, \quad (14d)$$

where

$$F^{(1)} = \text{div}_x[F_x^{(1)}] + \partial_y F_y^{(1)} + F_h^{(1)}, \quad (14e)$$

$$F_x^{(1)} = -\frac{2}{h} w \nabla_x u - \frac{2}{h} g \nabla_x u^{(1)} - \frac{2}{h^2} g w \nabla_x u - \frac{1}{h^2} g^2 \nabla_x u^{(1)} + \frac{h+y}{h} \nabla_x w \partial_y u + \frac{h+y}{h} \nabla_x g \partial_y u^{(1)} + \frac{h+y}{h^2} w \nabla_x g \partial_y u \\ + \frac{h+y}{h^2} g \nabla_x w \partial_y u + \frac{h+y}{h^2} g \nabla_x g \partial_y u^{(1)}, \quad (14f)$$

$$F_y^{(1)} = \frac{h+y}{h} \nabla_x w \cdot \nabla_x u + \frac{h+y}{h} \nabla_x g \cdot \nabla_x u^{(1)} + \frac{h+y}{h^2} w \nabla_x g \cdot \nabla_x u + \frac{h+y}{h^2} g \nabla_x w \cdot \nabla_x u + \frac{h+y}{h^2} g \nabla_x g \cdot \nabla_x u^{(1)} \\ - \frac{2(h+y)^2}{h^2} \nabla_x w \cdot \nabla_x g \partial_y u - \frac{(h+y)^2}{h^2} |\nabla_x g|^2 \partial_y u^{(1)}, \quad (14g)$$

and

$$F_h^{(1)} = \frac{1}{h} \nabla_x w \cdot \nabla_x u + \frac{1}{h} \nabla_x g \cdot \nabla_x u^{(1)} + \frac{1}{h^2} w \nabla_x g \cdot \nabla_x u + \frac{1}{h^2} g \nabla_x w \cdot \nabla_x u + \frac{1}{h^2} g \nabla_x g \cdot \nabla_x u^{(1)} \\ - \frac{2(h+y)}{h^2} \nabla_x w \cdot \nabla_x g \partial_y u - \frac{h+y}{h^2} |\nabla_x g|^2 \partial_y u^{(1)}. \quad (14h)$$

Next, the variation of the DNO satisfies the formula

$$G^{(1)}(g)[\xi]\{w\} = \partial_y u^{(1)}(x, 0) + H^{(1)}(x), \quad (15a)$$

where

$$H^{(1)} = -\frac{1}{h} w G(g)[\xi] - \frac{1}{h} g G^{(1)}(g)[\xi]\{w\} - \nabla_x w \cdot \nabla_x u(x, 0) - \nabla_x g \cdot \nabla_x u^{(1)}(x, 0) - \frac{1}{h} w \nabla_x g \cdot \nabla_x u(x, 0) \\ - \frac{1}{h} g \nabla_x w \cdot \nabla_x u(x, 0) - \frac{1}{h} g \nabla_x g \cdot \nabla_x u^{(1)}(x, 0) + 2 \nabla_x w \cdot \nabla_x g \partial_y u(x, 0) + |\nabla_x g|^2 \partial_y u^{(1)}(x, 0), \quad (15b)$$

c.f. [27].

With (12)–(15) in hand the TFE method now instructs us to make the following Taylor series expansions for the field and DNO

$$u(x, y, \varepsilon) = \sum_{n=0}^{\infty} u_n(x, y) \varepsilon^n, \quad G(\varepsilon f)[\xi] = \sum_{n=0}^{\infty} G_n(f)[\xi] \varepsilon^n, \quad (16)$$

and their first variations

$$u^{(1)}(x, y, \varepsilon) = \sum_{n=0}^{\infty} u_n^{(1)}(x, y) \varepsilon^n, \quad G^{(1)}(\varepsilon f)[\xi] = \sum_{n=0}^{\infty} G_n^{(1)}(f)[\xi] \varepsilon^n, \quad (17)$$

both of which can be shown to converge strongly in appropriate function spaces [23,25,27].

Upon insertion of (16) into (12), we find that the  $u_n$  must satisfy

$$\Delta u_n = F_n(x, y) \quad \text{in } S_{h,0}, \quad (18a)$$

$$u_n(x, 0) = \delta_{n,0} \xi(x), \quad (18b)$$

$$\partial_y u_n(x, -h) = 0, \quad (18c)$$

$$u_n(x + \gamma, y) = u_n(x, y) \quad \forall \gamma \in \Gamma, \quad (18d)$$

where  $\delta_{n,m}$  is the Kronecker delta,

$$F_n = \text{div}_x[F_{x,n}] + \partial_y F_{y,n} + F_{h,n}, \quad (18e)$$

$$F_{x,n} = -\frac{2}{h} f \nabla_x u_{n-1} - \frac{1}{h^2} f^2 \nabla_x u_{n-2} + \frac{h+y}{h} \nabla_x f \partial_y u_{n-1} + \frac{h+y}{h^2} f \nabla_x f \partial_y u_{n-2}, \quad (18f)$$

$$F_{y,n} = \frac{h+y}{h} \nabla_x f \cdot \nabla_x u_{n-1} + \frac{h+y}{h^2} f \nabla_x f \cdot \nabla_x u_{n-2} - \frac{(h+y)^2}{h^2} |\nabla_x f|^2 \partial_y u_{n-2}, \tag{18g}$$

and

$$F_{h,n} = \frac{1}{h} \nabla_x f \cdot \nabla_x u_{n-1} + \frac{1}{h^2} f \nabla_x f \cdot \nabla_x u_{n-2} - \frac{h+y}{h^2} |\nabla_x f|^2 \partial_y u_{n-2}. \tag{18h}$$

In these and future formulas any function with a negative index should be replaced by zero. Furthermore, the expansion of  $G$  inserted into (13) yields

$$G_n(f)[\xi] = \partial_y u_n(x, 0) + H_n(x), \tag{19a}$$

where

$$H_n = -\frac{1}{h} f G_{n-1}(f)[\xi] - \nabla_x f \cdot \nabla_x u_{n-1}(x, 0) - \frac{1}{h} f \nabla_x f \cdot \nabla_x u_{n-2}(x, 0) + |\nabla_x f|^2 \partial_y u_{n-2}(x, 0), \tag{19b}$$

see [23].

Finally, by putting (17) into (14), we discover that

$$\Delta u_n^{(1)} = F_n^{(1)}(x, y) \quad \text{in } S_{h,0}, \tag{20a}$$

$$u_n^{(1)}(x, 0) = 0, \tag{20b}$$

$$\partial_y u_n^{(1)}(x, -h) = 0, \tag{20c}$$

$$u_n^{(1)}(x + \gamma, y) = u_n^{(1)}(x, y) \quad \forall \gamma \in \Gamma, \tag{20d}$$

where

$$F_n^{(1)} = \text{div}_x [F_{x,n}^{(1)}] + \partial_y F_{y,n}^{(1)} + F_{h,n}^{(1)}, \tag{20e}$$

and

$$F_{x,n}^{(1)} = -\frac{2}{h} w \nabla_x u_n - \frac{2}{h} f \nabla_x u_{n-1}^{(1)} - \frac{2}{h^2} w f \nabla_x u_{n-1} - \frac{1}{h^2} f^2 \nabla_x u_{n-2}^{(1)} + \frac{h+y}{h} \nabla_x w \partial_y u_n + \frac{h+y}{h} \nabla_x f \partial_y u_{n-1}^{(1)} + \frac{h+y}{h^2} w \nabla_x f \partial_y u_{n-1} + \frac{h+y}{h^2} f \nabla_x w \partial_y u_{n-1} + \frac{h+y}{h^2} f \nabla_x f \partial_y u_{n-2}^{(1)}, \tag{20f}$$

$$F_{y,n}^{(1)} = \frac{h+y}{h} \nabla_x w \cdot \nabla_x u_n + \frac{h+y}{h} \nabla_x f \cdot \nabla_x u_{n-1}^{(1)} + \frac{h+y}{h^2} w \nabla_x f \cdot \nabla_x u_{n-1} + \frac{h+y}{h^2} f \nabla_x w \cdot \nabla_x u_{n-1} + \frac{h+y}{h^2} f \nabla_x f \cdot \nabla_x u_{n-2}^{(1)} - \frac{2(h+y)^2}{h^2} \nabla_x w \cdot \nabla_x f \partial_y u_{n-1} - \frac{(h+y)^2}{h^2} |\nabla_x f|^2 \partial_y u_{n-2}^{(1)}, \tag{20g}$$

and

$$F_{h,n}^{(1)} = \frac{1}{h} \nabla_x w \cdot \nabla_x u_n + \frac{1}{h} \nabla_x f \cdot \nabla_x u_{n-1}^{(1)} + \frac{1}{h^2} w \nabla_x f \cdot \nabla_x u_{n-1} + \frac{1}{h^2} f \nabla_x w \cdot \nabla_x u_{n-1} + \frac{1}{h^2} f \nabla_x f \cdot \nabla_x u_{n-2}^{(1)} - \frac{2(h+y)}{h^2} \nabla_x w \cdot \nabla_x f \partial_y u_{n-1} - \frac{h+y}{h^2} |\nabla_x f|^2 \partial_y u_{n-2}^{(1)}. \tag{20h}$$

In a similar fashion, the  $G_n^{(1)}$  can be computed via

$$G_n^{(1)}(f)[\xi]\{w\} = \partial_y u_n^{(1)}(x, 0) + H_n^{(1)}(x), \tag{21a}$$

where

$$H_n^{(1)} = -\frac{1}{h} w G_n(f)[\xi] - \frac{1}{h} f G_{n-1}^{(1)}(f)[\xi]\{w\} - \nabla_x w \cdot \nabla_x u_n(x, 0) - \nabla_x f \cdot \nabla_x u_{n-1}^{(1)}(x, 0) - \frac{1}{h} w \nabla_x f \cdot \nabla_x u_{n-1}(x, 0) - \frac{1}{h} f \nabla_x w \cdot \nabla_x u_{n-1}(x, 0) - \frac{1}{h} f \nabla_x f \cdot \nabla_x u_{n-2}^{(1)}(x, 0) + 2 \nabla_x w \cdot \nabla_x f \partial_y u_{n-1}(x, 0) + |\nabla_x f|^2 \partial_y u_{n-2}^{(1)}(x, 0), \tag{21b}$$

see [27].

#### 4. Numerical results

We are now in a position to compare the computational capabilities of the Operator Expansion (OE) recursions (28) to their Transformed Field Expansions (TFE) counterparts (21) for the simulation of the first variation of the Dirichlet–Neumann operator (DNO). For the numerical implementation of each method we follow the high-order/spectral philosophy of Craig

and Sulem [1] and Nicholls and Reitch [24]. These numerical simulations are then compared with a specially constructed exact solution which provides, for given Dirichlet data, the corresponding Neumann data. We test these numerical methods for a variety of surface deformations,  $g$ , and variation directions,  $w$ , with differing smoothness properties. As we shall see, while the OE method works well within its domain of applicability (small and regular deformations requiring only a small number of terms in the Taylor series of the variation of the DNO), the computation of higher order terms is unreliable. By contrast, our new TFE recursions can be robustly computed for any perturbation order leading to high-fidelity solutions for any choice of deformation or direction.

#### 4.1. Numerical method

As we mentioned above, we will follow a high-order/spectral philosophy to approximate the first variation of the DNO by both the OE and TFE methods. As we remarked in (10), we will approximate this variation,  $G^{(1)}$ , by the truncated Taylor series

$$G^{(1,N)}(\varepsilon f)[\xi]\{w\} := \sum_{n=0}^N G_n^{(1)}(f)[\xi]\{w\} \varepsilon^n.$$

For simplicity we will focus on the  $d = 2$  dimensional problem and further set the periodicity of our profiles to be  $L = 2\pi$ . In this case the OE method simulates each of the  $G_n^{(1)}$  by the truncated Fourier series

$$G_n^{(1)}(x) \approx G_{n,N_x}^{(1)} := \sum_{k=-N_x/2}^{N_x/2-1} \widehat{G}_n^{(1)}(k) e^{ikx}.$$

In (28) it is necessary to compute not only classical derivatives, e.g.  $D$ , but also Fourier multipliers such as  $|D|^m$ . Both are easily accomplished via the Discrete Fourier Transform (DFT) algorithm, accelerated by the Fast Fourier Transform (FFT), as all of these operators can be applied pointwise to the Fourier coefficients of the relevant functions. Products appearing in (28) are accomplished via the (inverse) DFT and pointwise multiplication in physical space.

The specification for the TFE method is somewhat more involved as a discretization in the vertical,  $y$ , direction is required for both the field and its first variation. Thus, we approximate  $u$  and  $u^{(1)}$  by

$$u_{n,N_x,N_y}(x,y) := \sum_{l=0}^{N_y} \sum_{k=-N_x/2}^{N_x/2-1} \hat{u}_n(k,l) T_l\left(\frac{2y+h}{h}\right) e^{ikx}, \quad (22a)$$

$$u_{n,N_x,N_y}^{(1)}(x,y) := \sum_{l=0}^{N_y} \sum_{k=-N_x/2}^{N_x/2-1} \hat{u}_n^{(1)}(k,l) T_l\left(\frac{2y+h}{h}\right) e^{ikx}, \quad (22b)$$

where  $T_l$  is the  $l$ th Chebyshev polynomial, and, again,

$$G_n^{(1)}(x) \approx G_{n,N_x}^{(1)} := \sum_{k=-N_x/2}^{N_x/2-1} \widehat{G}_n^{(1)}(k) e^{ikx}.$$

Upon insertion of (22) into (20) we realize that a two-point boundary value problem must be solved (c.f. [24]) which we accomplish with a Chebyshev tau approach [31,32]. After this is accomplished then all other derivatives and multiplications are completed with the standard approach of DFT/DCT (Discrete Chebyshev transform) coupled to pointwise multiplication on either the Fourier/Chebyshev or physical side. As with the computation of DNO, the operation counts are

$$\mathcal{O}(N_x \log(N_x)N), \quad \mathcal{O}(N_x \log(N_x)N_y \log(N_y)N),$$

for the OE and TFE methods, respectively. While disadvantaged in terms of computational complexity versus the OE algorithm, the TFE method is mandated for profiles too large and/or too rough for the OE formulation (see Figs. 1–11).

To test our numerical simulations we take advantage of the fact that it is very easy to build a class of exact solutions for the DNO problem, and thus the first variation of the DNO. As was described in [24], consider the function

$$u_k(x,y) := \cosh(|k|(y+h)) e^{ikx}, \quad k \in \mathbf{Z}.$$

This function satisfies (2a), (2c) and (2d), and if we now choose a boundary deformation  $g(x)$  we can specify Dirichlet data

$$\xi_k(x) := \cosh(|k|(g+h)) e^{ikx},$$

which has the exact Neumann data:

$$v_k(x) := (\partial_y u_k - (\partial_x g) \partial_x u_k)_{y=g(x)} = \{|k| \sinh(|k|(g+h)) - (\partial_x g)(ik) \cosh(|k|(g+h))\} e^{ikx}.$$

With this  $\{\xi_k, v_k\}$  pair it is now easy to test the convergence of simulations of the DNO. For the first variation of the DNO we have that

$$v_k^{(1)}\{w\} := \lim_{\tau \rightarrow 0} \frac{1}{\tau} (v_k(x; g + \tau w) - v_k(x; g))$$

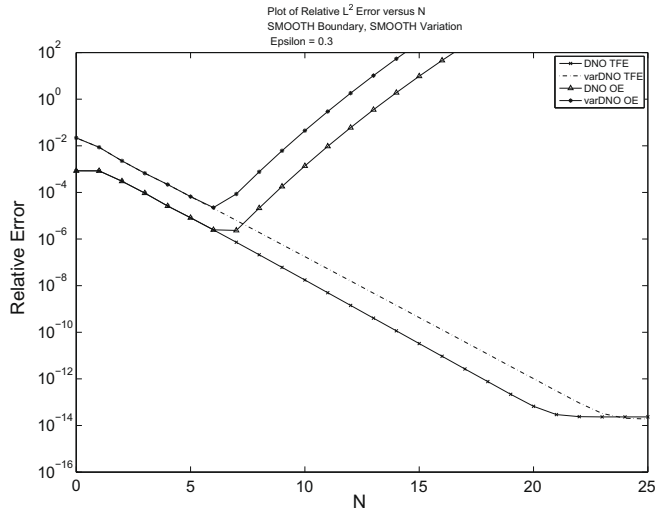


**Fig. 1.** Plot of relative  $L^2$  error for the OE and TFE methods in the computation of the first variation of the DNO with smooth deformation, (23a), and smooth direction, (24a). The numerical parameters were  $N_x = 256$ ,  $N_y = 64$ ,  $N = 40$ , and  $\varepsilon = 0.3$ .

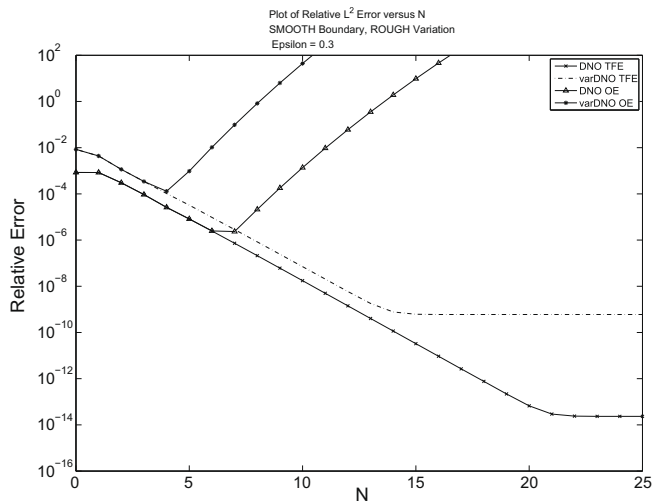


**Fig. 2.** Plot of relative  $L^2$  error for the OE and TFE methods in the computation of the first variation of the DNO with smooth deformation, (23a), and rough direction, (24b). The numerical parameters were  $N_x = 256$ ,  $N_y = 64$ ,  $N = 40$ , and  $\varepsilon = 0.3$ .

which is easily computed as

$$v_k^{(1)}\{w\} = \{|k|^2 \cosh(|k|(g+h))w - (\partial_x w)(ik) \cosh(|k|(g+h)) - (\partial_x g)(ik)|k| \sinh(|k|(g+h))w\}e^{ikx}.$$

It would seem that we are ready to proceed to the testing of our new algorithms save for a subtle observation: For this example the Dirichlet data *does* depend explicitly upon  $g$ . Thus, to be careful we write the relationship

$$G(g)[\xi_k(x; g)] = v_k(x; g);$$

differentiating with respect to  $g$  we find

$$G^{(1)}(g)[\xi_k(x; g)]\{w\} + G(g)[\xi_k^{(1)}(x; g)\{w\}] = v_k^{(1)}(x; g)\{w\}.$$

Thus, to complete our study we need

$$\xi_k^{(1)}\{w\} = |k| \sinh(|k|(g+h))we^{ikx},$$



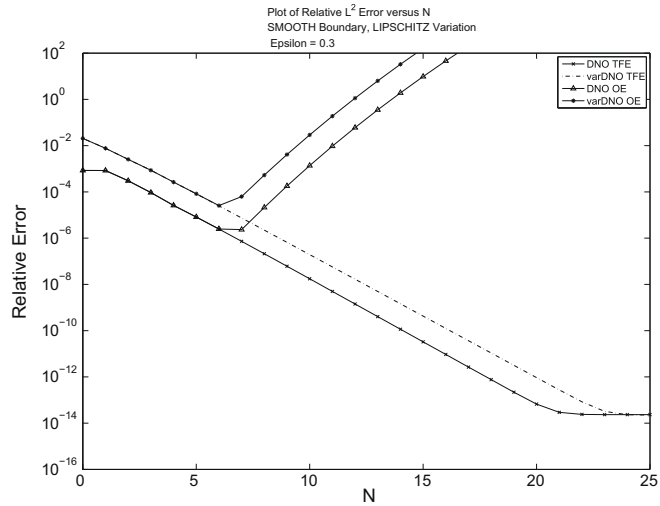


**Fig. 3.** Plot of relative  $L^2$  error for the OE and TFE methods in the computation of the first variation of the DNO with smooth deformation, (23a), and Lipschitz direction, (24c). The numerical parameters were  $N_x = 256$ ,  $N_y = 64$ ,  $N = 40$ , and  $\varepsilon = 0.3$ .

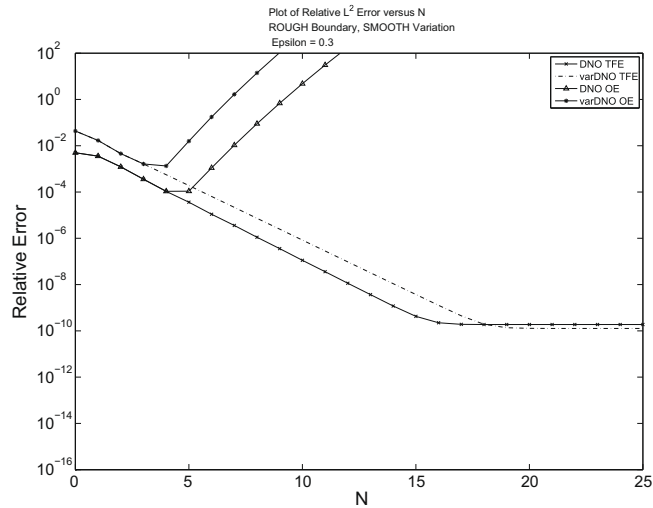


**Fig. 4.** Plot of relative  $L^2$  error for the OE and TFE methods in the computation of the first variation of the DNO with rough deformation, (23b), and smooth direction, (24a). The numerical parameters were  $N_x = 256$ ,  $N_y = 64$ ,  $N = 40$ , and  $\varepsilon = 0.3$ .

and thus

$$G^{(1)}(\mathbf{g})[\xi_k(\mathbf{x}; \mathbf{g})]\{\mathbf{w}\} = v_k^{(1)}(\mathbf{x}; \mathbf{g})\{\mathbf{w}\} - G(\mathbf{g})[\xi^{(1)}(\mathbf{x}; \mathbf{g})\{\mathbf{w}\}]$$

is our exact solution.

#### 4.2. Results

Before presenting our results we state the families of profiles,  $\mathbf{g} = \varepsilon f$ , and variation directions,  $\mathbf{w}$ , employed in our numerical studies. As we shall see, the performance of both the OE and TFE methods depend upon the smoothness of the underlying profiles. For this reason we have selected three profiles

$$f_s(\mathbf{x}) = \sin(\mathbf{x}), \tag{23a}$$

$$f_r(\mathbf{x}) = A\mathbf{x}^4(2\pi - \mathbf{x})^4 + B, \tag{23b}$$

$$f_L(\mathbf{x}) = \begin{cases} -(\frac{2}{\pi})\mathbf{x} + 1 & \mathbf{x} \in [0, \pi), \\ (\frac{2}{\pi})\mathbf{x} - 3 & \mathbf{x} \in [\pi, 2\pi), \end{cases} \tag{23c}$$

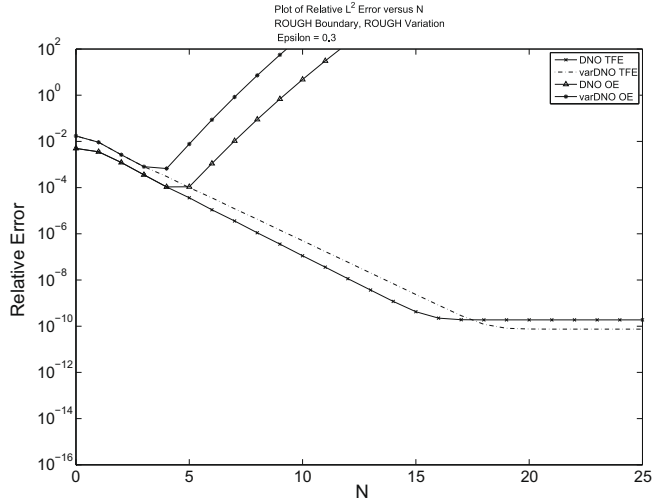


**Fig. 5.** Plot of relative  $L^2$  error for the OE and TFE methods in the computation of the first variation of the DNO with rough deformation, (23b), and rough direction, (24b). The numerical parameters were  $N_x = 256$ ,  $N_y = 64$ ,  $N = 40$ , and  $\varepsilon = 0.3$ .

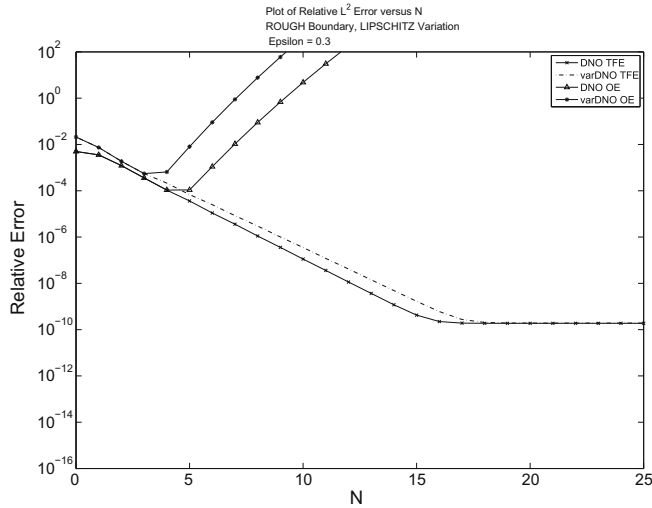


**Fig. 6.** Plot of relative  $L^2$  error for the OE and TFE methods in the computation of the first variation of the DNO with rough deformation, (23b), and Lipschitz direction, (24c). The numerical parameters were  $N_x = 256$ ,  $N_y = 64$ ,  $N = 40$ , and  $\varepsilon = 0.3$ .

belonging to three quite different function spaces. The first,  $f_s$ , is “smooth” (in fact analytic), the second,  $f_r$ , is  $C^4$  (“rough”), while the third,  $f_l$ , is Lipschitz. In a similar fashion we have chosen three directions

$$w_s(x) = -\sin(2x), \tag{24a}$$

$$w_r(x) = A'x^3(2\pi - x)^3 + B', \tag{24b}$$

$$w_l(x) = \frac{3}{2} \begin{cases} -(\frac{2}{\pi})x + \frac{1}{2} & x \in [0, \pi/2), \\ (\frac{2}{\pi})x - \frac{3}{2} & x \in [\pi/2, \pi), \\ -(\frac{2}{\pi})x + \frac{5}{2} & x \in [\pi, 3\pi/2), \\ (\frac{2}{\pi})x - \frac{7}{2} & x \in [3\pi/2, 2\pi). \end{cases} \tag{24c}$$

Again, these correspond to “smooth,” “rough” ( $C^3$ ), and Lipschitz profiles. The constants  $A, A', B, B'$  are chosen so that the functions have zero mean and  $\mathcal{O}(1)$  amplitude and slope.

At this point we display results of OE and TFE simulations of the DNO and its first variation using the truncated Taylor series (9) and (10) via (26), (19), (28), and (21). In all of these runs we set  $N_x = 256, N_y = 64$  (for the TFE method), and

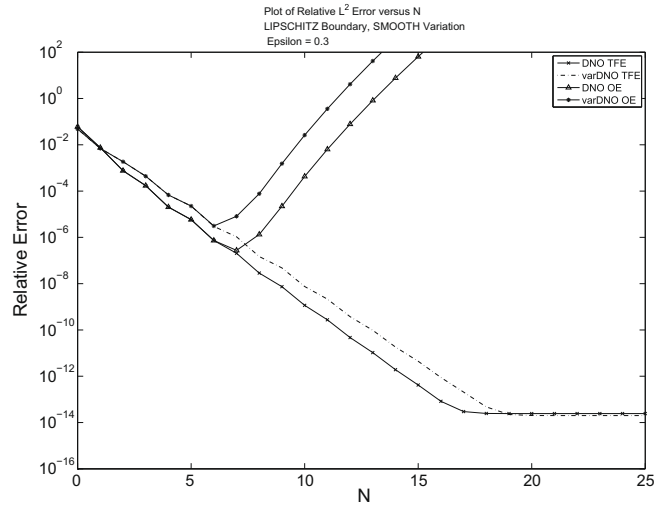


**Fig. 7.** Plot of relative  $L^2$  error for the OE and TFE methods in the computation of the first variation of the DNO with Lipschitz deformation, (23c), and smooth direction, (24a). The numerical parameters were  $N_x = 256$ ,  $N_y = 64$ ,  $N = 40$ , and  $\varepsilon = 0.3$ .

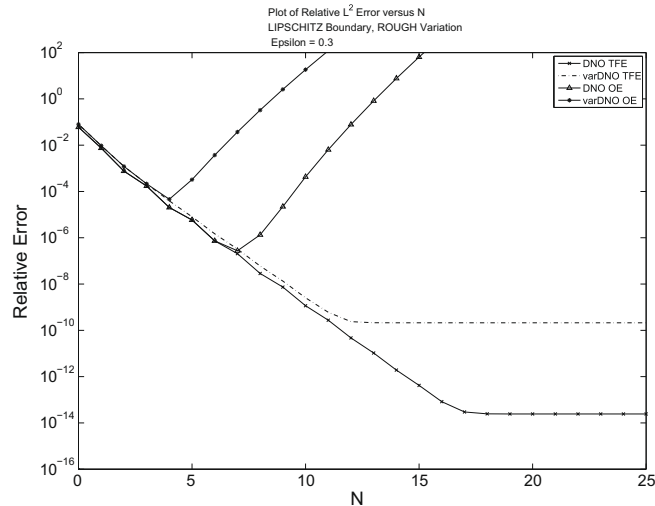


**Fig. 8.** Plot of relative  $L^2$  error for the OE and TFE methods in the computation of the first variation of the DNO with Lipschitz deformation, (23c), and rough direction, (24b). The numerical parameters were  $N_x = 256$ ,  $N_y = 64$ ,  $N = 40$ , and  $\varepsilon = 0.3$ .

$N = 40$ , and to minimize the effects of aliasing the Fourier representations of all profiles  $f$  and directions  $w$  were truncated beyond wavenumber 20. Furthermore, the common perturbation value of  $\varepsilon = 0.3$  was utilized for all simulations.

In Fig. 1 we see that, for a smooth deformation  $f_s$  and a smooth direction  $w_s$ , both the OE and TFE methods deliver reliable results through the first six perturbation orders. However, beyond the seventh order the performance of the OE recursions deteriorate while the TFE method continues to improve (all the way to nearly machine precision by  $N = 23$ ). In Figs. 2 and 3 we see similar behavior for the case of the smooth deformation,  $f_s$ , and rough,  $w_r$ , and Lipschitz,  $w_L$ , directions, respectively. Again, the OE methodology gives excellent results through four and six perturbation orders respectively before diverging, while the TFE recursions continue to improve as the perturbation orders increase (again giving nearly machine precision for some  $N \approx 22, 23$ ).

In Figs. 4–6 we repeat these experiments with the  $C^4$  deformation,  $f_r$ , and smooth,  $C^3$ , and Lipschitz directions, respectively. We notice very similar behavior to that observed in the smooth deformation case. Excellent convergence of both algorithms though three perturbation orders followed by divergence of the OE method compared with persistent convergence of the TFE recursions eventually approaching machine precision.

Finally, in Figs. 7–9 we conduct the same experiments with the Lipschitz deformation,  $f_L$ , and smooth,  $C^3$ , and Lipschitz directions, respectively. The computational properties of the OE and TFE algorithms are much the same in this case save that the divergence of OE occurs for a *slightly* larger value of  $n$ .

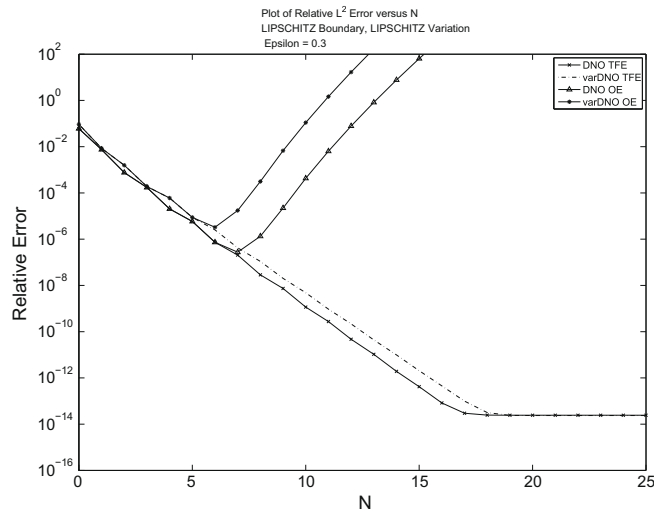


**Fig. 9.** Plot of relative  $L^2$  error for the OE and TFE methods in the computation of the first variation of the DNO with Lipschitz deformation, (23c), and Lipschitz direction, (24c). The numerical parameters were  $N_x = 256$ ,  $N_y = 64$ ,  $N = 40$ , and  $\varepsilon = 0.3$ .

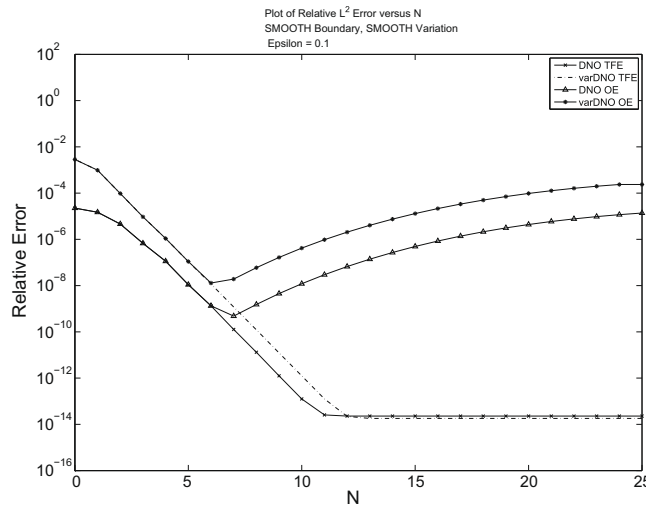


**Fig. 10.** Plot of relative  $L^2$  error for the OE and TFE methods in the computation of the first variation of the DNO with smooth deformation, (23a), and smooth direction, (24a). The numerical parameters were  $N_x = 256$ ,  $N_y = 64$ ,  $N = 40$ , and  $\varepsilon = 0.1$ .

**Remark 1.** Regarding the choice of the vertical discretization parameter  $N_y$ , for all of the results presented here  $N_y = 64$  was sufficient to resolve the solution in the vertical direction and thus we retained this value for consistency. However, if the depth of the fluid were increased drastically this value would no longer suffice and a larger one must be selected. One method for avoiding this issue (which we do not pursue in this paper) is to introduce an “Artificial Boundary” to the problem (see, e.g., [33]) at  $y = a$  below the lowest point of the traveling wave, but well above the bottom of the fluid. One of the authors in collaboration with F. Reitich (Nicholls and Reitich [33]) showed how this could be accomplished with an exact boundary condition at  $y = a$ . In this way the problem domain can be significantly reduced allowing a moderate choice of  $N_y$  irrespective of fluid depth.

**Remark 2.** The rate of convergence of these Boundary Perturbation methods generally depend upon the size and/or smoothness of the problem domain. Such smoothness effects are evident in Figs. 1–9, though the smoothness of the boundary plays a stronger role than that of the direction as the latter only appears linearly while the former in a very nonlinear fashion. To investigate the role of deformation size as well as roughness we consider the convergence experiments described above in two “extreme” cases: Very smooth and small perturbation, and very rough and large perturbation. The results of this experiment for a smooth deformation, a smooth direction, and a rather small value of  $\varepsilon = 0.1$  appear in Fig. 10. Here we see that

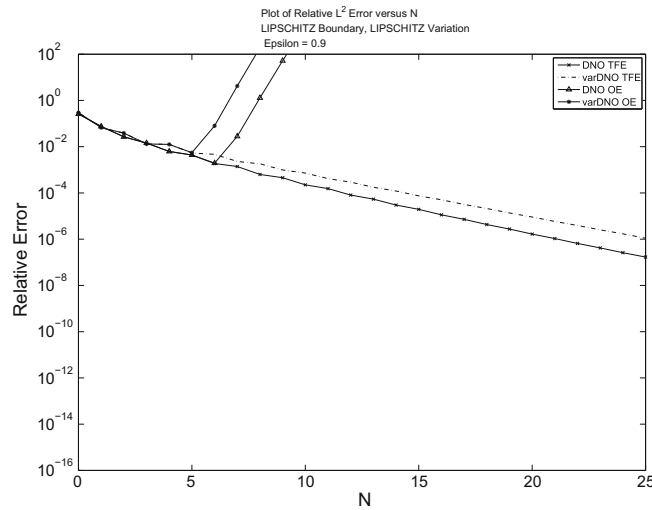


**Fig. 11.** Plot of relative  $L^2$  error for the OE and TFE methods in the computation of the first variation of the DNO with Lipschitz deformation, (23c), and Lipschitz direction, (24c). The numerical parameters were  $N_x = 256$ ,  $N_y = 64$ ,  $N = 40$ , and  $\varepsilon = 0.9$ .

the relative errors realized by the OE algorithm are *far* smaller (roughly  $10^{-8}$ ) than those seen at  $\varepsilon = 0.3$  (about  $10^{-5}$ , see Fig. 1). The outcome in the case of a Lipschitz deformation, a Lipschitz direction, and a large value of  $\varepsilon = 0.9$  are depicted in Fig. 11. In this case we see that the relative errors delivered by the OE algorithm are *significantly* larger (roughly  $10^{-2}$ ) than those seen at  $\varepsilon = 0.3$  (about  $10^{-5}$ , see Fig. 9).

**5. Conclusions**

In this paper we have presented a novel, stable, and highly accurate method for the simulation of the first variation of the Dirichlet–Neumann operator. We compared the numerical properties of this Transformed Field Expansions method with another popular Boundary Perturbation approach, the method of Operator Expansions, for a variety of boundary shapes and variation directions. While the details of these experiments vary as the shape or direction is changed, the general conclusions are the same. The classical Operator Expansions method gives accurate answers for a certain number of perturbation orders, before divergence sets in. By contrast, our new Transformed Field Expansions method delivers errors which are never worse than those produced by Operator Expansions, while significantly improving on this method for higher perturbation orders. In fact, provided that enough perturbation orders are retained, machine accuracy can always be attained with our new method.

**Acknowledgment**

DPN gratefully acknowledges support from the NSF through Grant No. DMS-0810958.

**Appendix A. Operator Expansions**

In this appendix we give a brief overview of the derivation of the Operator Expansions (OE) method for computing the  $G_n$  and  $G_n^{(1)}$  in the expansions of the DNO and its first variation (see (7) and (8)). Consider the functions

$$v_k(x, y) = \cosh(|k|(y + h))e^{ikx}, \quad k \in \Gamma',$$

which satisfy Eqs. (2a), (2c) and (2d) of the elliptic problem which defines the DNO. From the definition of the DNO, (3), we have

$$G(\varepsilon f)[\cosh(|k|(\varepsilon f + h))e^{ikx}] = (\partial_y - \varepsilon \nabla_x f \cdot \nabla_x)(\cosh(|k|(y + h))e^{ikx})_{y=\varepsilon f}. \tag{25}$$

Expanding the DNO,  $G$ , and the exponentials in the equation above in a power series in  $\varepsilon$ , we obtain expressions for the  $G_n$ . In the case  $n = 0$  we recover

$$G_0[e^{ikx}] = |k| \tanh(h|k|)e^{ikx} = |D| \tanh(h|D|)e^{ikx},$$

using the Fourier multiplier notation  $D := (1/i)\nabla_x$ . As generic  $L^2$  functions can be uniquely expressed in terms of their Fourier series we identify

$$G_0[\xi] = \sum_{k \in \Gamma'} |k| \tanh(h|k|) \hat{\xi}_k e^{ikx} = |D| \tanh(h|D|) \xi.$$

This can be extended to higher orders resulting in the following formulas (c.f. [1,6]). For odd numbered terms  $n = 2j - 1 > 0$ , we have:

$$G_{2j-1}(f) = \frac{1}{(2j-1)!} D \cdot f^{2j-1} D |D|^{2(j-1)} - \sum_{s=0}^{j-1} \frac{1}{(2(j-s)-1)!} G_{2s}(f) [f^{2(j-s)-1} |D|^{2(j-s-1)} G_0] - \sum_{s=0}^{j-2} \frac{1}{(2(j-s-1))!} G_{2s+1}(f) [f^{2(j-s-1)} |D|^{2(j-s-1)}].$$

For even numbered terms  $n = 2j > 0$ :

$$G_{2j}(f) = \frac{1}{(2j)!} D \cdot f^{2j} D |D|^{2(j-1)} G_0 - \sum_{s=0}^{j-1} \frac{1}{(2(j-s))!} G_{2s}(f) [f^{2(j-s)} |D|^{2(j-s)}] - \sum_{s=0}^{j-1} \frac{1}{(2(j-s)-1)!} G_{2s+1}(f) [f^{2(j-s)-1} |D|^{2(j-s-1)} G_0].$$

Self-adjointness properties of the DNO, e.g.,

$$G^* = G, \quad G_n^* = G_n, \quad |D|^* = |D|,$$

allow us write these as

$$G_0 = |D| \tanh(h|D|), \tag{26a}$$

$$G_{2j-1}(f) = \frac{1}{(2j-1)!} |D|^{2(j-1)} D \cdot f^{2j-1} D - \sum_{s=0}^{j-1} \frac{1}{(2(j-s)-1)!} G_0 |D|^{2(j-s-1)} f^{2(j-s)-1} G_{2s}(f) - \sum_{s=0}^{j-2} \frac{1}{(2(j-s-1))!} |D|^{2(j-s-1)} f^{2(j-s-1)} G_{2s+1}(f), \tag{26b}$$

$$G_{2j}(f) = \frac{1}{(2j)!} G_0 |D|^{2(j-1)} D \cdot f^{2j} D - \sum_{s=0}^{j-1} \frac{1}{(2(j-s))!} |D|^{2(j-s)} f^{2(j-s)} G_{2s}(f) - \sum_{s=0}^{j-1} \frac{1}{(2(j-s)-1)!} G_0 |D|^{2(j-s-1)} f^{2(j-s)-1} G_{2s+1}(f). \tag{26c}$$

To find the first variation of the DNO from this OE philosophy we formally differentiate the expansion

$$G(g) = \sum_{n=0}^{\infty} G_n(g),$$

c.f. (7), with respect to  $g$  which yields

$$G^{(1)}(g)\{w\} = \delta_g G(g)\{w\} = \sum_{n=0}^{\infty} (\delta_g G_n)(g)\{w\}. \tag{27}$$

If we now set  $g = \epsilon f$  then, from [27], we obtain

$$G^{(1)}(\epsilon f)\{w\} = \sum_{n=0}^{\infty} G_n^{(1)}(f)\{w\} \epsilon^n.$$

Comparing this with (27) we identify

$$G_n^{(1)}(f) = (\delta_g G_{n+1})(f)$$

upon noting that, due to the variation,

$$(\delta_g G_n)(\epsilon f) = (\delta_g G_n)(f) \epsilon^{n-1}.$$

Thus, for  $j \geq 1$ ,

$$G_{2j-2}^{(1)}(f)\{w\} = (\delta_g G_{2j-1})(f)\{w\} = \frac{1}{(2(j-1))!} |D|^{2(j-1)} D \cdot f^{2(j-1)} w D - \sum_{s=0}^{j-1} \frac{1}{(2(j-s-1))!} G_0 |D|^{2(j-s-1)} f^{2(j-s-1)} w G_{2s}(f) - \sum_{s=0}^{j-1} \frac{1}{(2(j-s)-1)!} G_0 |D|^{2(j-s-1)} f^{2(j-s)-1} G_{2s}^{(1)}(f) - \sum_{s=0}^{j-2} \frac{1}{(2(j-s-1)-1)!} |D|^{2(j-s-1)} f^{2(j-s-1)-1} w G_{2s+1}(f) - \sum_{s=0}^{j-2} \frac{1}{(2(j-s-1))!} |D|^{2(j-s-1)} f^{2(j-s-1)} G_{2s+1}^{(1)}(f), \tag{28a}$$

and, for  $j \geq 1$ ,

$$\begin{aligned} G_{2j-1}^{(1)}(f)\{w\} &= (\delta_g G_{2j})(f)\{w\} = \frac{1}{(2j-1)!} G_0 |D|^{2(j-1)} D \cdot f^{2j-1} w D - \sum_{s=0}^{j-1} \frac{1}{(2(j-s)-1)!} |D|^{2(j-s)} f^{2(j-s)-1} w G_{2s}(f) \\ &\quad - \sum_{s=0}^{j-1} \frac{1}{(2(j-s))!} |D|^{2(j-s)} f^{2(j-s)} G_{2s}^{(1)}(f) - \sum_{s=0}^{j-1} \frac{1}{(2(j-s-1))!} G_0 |D|^{2(j-s-1)} f^{2(j-s-1)} w G_{2s+1}(f) \\ &\quad - \sum_{s=0}^{j-1} \frac{1}{(2(j-s)-1)!} G_0 |D|^{2(j-s-1)} f^{2(j-s)-1} G_{2s+1}^{(1)}(f). \end{aligned} \quad (28b)$$

## References

- [1] W. Craig, C. Sulem, Numerical simulation of gravity waves, *J. Comput. Phys.* 108 (1993) 73–83.
- [2] F. Ihlenburg, *Finite Element Analysis of Acoustic Scattering*, Springer-Verlag, New York, 1998.
- [3] P.J. Kaczkowski, E.I. Thorsos, Application of the operator expansion method to scattering from one-dimensional moderately rough Dirichlet random surfaces, *J. Acoust. Soc. Am.* 96 (2) (1994) 957–972.
- [4] H. Lamb, *Hydrodynamics*, sixth ed., Cambridge University Press, Cambridge, 1993.
- [5] V. Zakharov, Stability of periodic waves of finite amplitude on the surface of a deep fluid, *J. Appl. Mech. Tech. Phys.* 9 (1968) 190–194.
- [6] D.P. Nicholls, Traveling water waves: spectral continuation methods with parallel implementation, *J. Comput. Phys.* 143 (1) (1998) 224–240.
- [7] D.P. Nicholls, On hexagonal gravity water waves, *Math. Comput. Simulat.* 55 (4–6) (2001) 567–575.
- [8] D.P. Nicholls, Spectral stability of traveling water waves: analytic dependence of the spectrum, *J. Nonlinear Sci.* 17 (4) (2007) 369–397.
- [9] D.P. Nicholls, Spectral data for traveling water waves: singularities and stability, *J. Fluid Mech.* 624 (2009) 339–360.
- [10] D.M. Milder, An improved formalism for rough-surface scattering of acoustic and electromagnetic waves, in: *Proceedings of SPIE – The International Society for Optical Engineering* (San Diego, 1991), *Int. Soc. for Optical Engineering*, vol. 1558, Bellingham, WA, 1991, pp. 213–221.
- [11] D.M. Milder, An improved formalism for wave scattering from rough surfaces, *J. Acoust. Soc. Am.* 89 (2) (1991) 529–541.
- [12] D.M. Milder, H.T. Sharp, An improved formalism for rough surface scattering. II. Numerical trials in three dimensions, *J. Acoust. Soc. Am.* 91 (5) (1992) 2620–2626.
- [13] W. Craig, P. Guyenne, J. Hammack, D. Henderson, C. Sulem, Solitary water wave interactions, *Phys. Fluids* 18 (5) (2006) 057106, 25.
- [14] P. Guyenne, D.P. Nicholls, Numerical simulation of solitary waves on plane slopes, *Math. Comput. Simulat.* 69 (2005) 269–281.
- [15] P. Guyenne, D.P. Nicholls, A high-order spectral method for nonlinear water waves over bottom topography, *SIAM J. Sci. Comput.* 30 (1) (2007) 81–101.
- [16] L. Rayleigh, On the dynamical theory of gratings, *Proc. Roy. Soc. London A79* (1907) 399–416.
- [17] S.O. Rice, Reflection of electromagnetic waves from slightly rough surfaces, *Commun. Pure Appl. Math.* 4 (1951) 351–378.
- [18] O.P. Bruno, F. Reitich, Numerical solution of diffraction problems: a method of variation of boundaries, *J. Opt. Soc. Am. A* 10 (6) (1993) 1168–1175.
- [19] O.P. Bruno, F. Reitich, Numerical solution of diffraction problems: a method of variation of boundaries. II. Finitely conducting gratings, Padé approximants, and singularities, *J. Opt. Soc. Am. A* 10 (11) (1993) 2307–2316.
- [20] O.P. Bruno, F. Reitich, Numerical solution of diffraction problems: a method of variation of boundaries. III. Doubly periodic gratings, *J. Opt. Soc. Am. A* 10 (12) (1993) 2551–2562.
- [21] O.P. Bruno, F. Reitich, Calculation of electromagnetic scattering via boundary variations and analytic continuation, *Appl. Comput. Electromagn. Soc. J.* 11 (1) (1996) 17–31.
- [22] O.P. Bruno, F. Reitich, Boundary-variation solutions for bounded-obstacle scattering problems in three dimensions, *J. Acoust. Soc. Am.* 104 (5) (1998) 2579–2583.
- [23] D.P. Nicholls, F. Reitich, A new approach to analyticity of Dirichlet–Neumann operators, *Proc. Roy. Soc. Edinburgh Sect. A* 131 (6) (2001) 1411–1433.
- [24] D.P. Nicholls, F. Reitich, Stability of high-order perturbative methods for the computation of Dirichlet–Neumann operators, *J. Comput. Phys.* 170 (1) (2001) 276–298.
- [25] D.P. Nicholls, F. Reitich, Analytic continuation of Dirichlet–Neumann operators, *Numer. Math.* 94 (1) (2003) 107–146.
- [26] F. Reitich, K. Tamma, State-of-the-art, trends, and directions in computational electromagnetics, *CMES Comput. Model. Eng. Sci.* 5 (4) (2004) 287–294.
- [27] C. Fazioli, D.P. Nicholls, Parametric analyticity of functional variations of Dirichlet–Neumann operators, *Diff. Int. Eq.* 21 (5–6) (2008) 541–574.
- [28] A.P. Calderón, Cauchy integrals on Lipschitz curves and related operators, *Proc. Nat. Acad. Sci. USA* 75 (1977) 1324–1327.
- [29] R. Coifman, Y. Meyer, Nonlinear harmonic analysis and analytic dependence, in: *Pseudo differential operators and applications*, Notre Dame, Ind., 1984, Amer. Math. Soc., 1985, pp. 71–78.
- [30] W. Craig, U. Schanz, C. Sulem, The modulation regime of three-dimensional water waves and the Davey–Stewartson system, *Ann. Inst. Henri Poincaré* 14 (1997) 615–667.
- [31] D. Gottlieb, S.A. Orszag, Numerical analysis of spectral methods: theory and applications, in: *CBMS-NSF Regional Conference Series in Applied Mathematics*, No. 26, Society for Industrial and Applied Mathematics, Philadelphia, PA, 1977.
- [32] C. Canuto, M.Y. Hussaini, A. Quarteroni, T.A. Zang, *Spectral Methods in Fluid Dynamics*, Springer-Verlag, New York, 1988.
- [33] D.P. Nicholls, F. Reitich, Rapid, stable, high-order computation of traveling water waves in three dimensions, *Eur. J. Mech. B Fluids* 25 (4) (2006) 406–424.